Journal of Computational Physics 228 (2009) 3891–3910

Contents lists available at ScienceDirect

Journal of Computational Physics

journal homepage: www.elsevier.com/locate/jcp

Fictitious Domain approach with *hp*-finite element approximation for incompressible fluid flow

Lucia Parussini *, Valentino Pediroda

Mechanical Engineering Department, University of Trieste, Via Valerio 10 (Bui.C5), 34127 Trieste, Italy

ARTICLE INFO

Article history:
Received 6 August 2008
Received in revised form 12 February 2009
Accepted 22 February 2009
Available online 28 February 2009

Keywords:
Fictitious Domain approach
Lagrange multipliers
Least Squares Spectral Element Method
Navier–Stokes equations

ABSTRACT

We consider the application of Fictitious Domain approach combined with least squares spectral elements for the numerical solution of fluid dynamic incompressible equations. Fictitious Domain methods allow problems formulated on a complicated shaped domain Ω to be solved on a simpler domain Π containing Ω. Least Squares Spectral Element Method has been used to develop the discrete model, as this scheme combines the generality of finite element methods with the accuracy of spectral methods. Moreover the least squares methods have theoretical and computational advantages in the algorithmic design and implementation. This paper presents the formulation and validation of the Fictitious Domain Least Squares Spectral Element approach for the steady incompressible Navier–Stokes equations. The convergence of the approximated solution is verified solving two-dimensional benchmark problems, demonstrating the predictive capability of the proposed formulation.

1. Introduction

Mathematical models used for describing the behavior of natural and manmade systems are usually based on partial differential equations (PDEs) that typically give the rate of change both in time and space of physical conservative quantities, such as mass, momentum and energy. Numerical solution of systems of PDEs is useful to reproduce past and predict future behavior of the system for a better understanding of the underlying mechanisms. One of the more difficult tasks for an efficient numerical solution of PDEs is the discretization of the model into finite elements or volumes. Typically this operation is time-consuming and the accuracy of numerical solution is strongly dependent on the quality of the mesh.

In this sense the Fictitious Domain approach, which is the formulation we propose in this paper, presents a great advantage. It is a methodology for numerical resolution of differential problems where the mesh is simple to construct and there is no need to create a different mesh for each new geometry of the problem. In fact the Fictitious Domain method allows problems formulated on a complicated shaped domain Ω to be solved on a simpler domain Π containing Ω. The extension of the original problem to the fictitious region Π/Ω must be chosen so that the solution of the extended problem restricted to Ω coincides with the solution of the original problem. The Fictitious Domain approach, where extended problem is defined on a simple domain, enables the use of efficient Cartesian grids.

It is easy to understand the appeal of such kind of approach for numerical simulations which involve changing geometries, i.e. flow with moving bodies, shape optimization problems, elastic structures, etc. An innovative application of the Fictitious Domain approach can be found in Parussini and Pediroda [1,2] where it has been used together with Polynomial Chaos methodologies for the study of geometric uncertainties.

* Corresponding author.
E-mail addresses: lparussini@units.it (L. Parussini), pediroda@units.it (V. Pediroda).

0021-9991/$ - see front matter © 2009 Elsevier Inc. All rights reserved.
doi:10.1016/j.jcp.2009.02.019

Actually the Fictitious Domain method is not itself a novelty. Literature on Fictitious Domain methods goes back to the 60s [3]. In the following years there has been an increasing interest on this kind of methodologies. So that several approaches have been developed to implement immersed conditions and we can find different applications: to acoustics [4–6], fluid dynamics [7,8], bio-medical problems [9–11]. Many methods have been introduced such as the Boundary Lagrangian method [12–14], Distributed Lagrangian method [8,11,15,16], Immersed Boundary method [17], Immersed Continuum method [18], Immersed Interface method [19], Fat Boundary method [20], Elimination method [21], Penalty method [22] and Immersed Finite Element method [23]. Although many methods have been proposed in a finite element, finite difference or finite volume context only few publications exist on the performance of non-matching approaches for high-order discretizations such as the spectral/*hp* element method. The spectral/*hp* approximation is based on higher-order functions, locally defined over finite size parts of domain. The advantage of such kind of method, in comparison with traditional finite element method, is its exponential convergence property with the increasing of polynomial order p, if the exact solution is sufficiently smooth.

A first example of Fictitious Domain approach with higher-order discretizations can be found in Dong et al. [24], where the Fictitious Domain method, as exploited by Glowinski et al. [25] in a finite element code, has been explored for a spectral/*hp* framework. A distributed Lagrange multiplier was used to couple the object to the underlying fluid. Exponential p-convergence was demonstrated for a Fictitious Domain approach with overlapping fluid domains and further performance was tested using the exact solution for a Wannier flow (Stokes flow) and using the flow around a cylinder (Navier–Stokes).

Another example is represented by Parussini [26], which is a first attempt of the authors of the present paper to develop a coupled methodology Fictitious Domain-Spectral Element Method (FD-SEM). The method was applied to heat conduction problems.

The new approach, we present in this paper, is the coupling of Fictitious Domain according to Boundary Lagrangian approach [12] together with the Least Squares Spectral Element Method (LSqSEM) [27,28]. We exploit the LSqSEM, which combines the least-squares formulation with a spectral element approximation. This provides several advantages. The LSqSEM produces symmetric positive definite linear systems for every type of partial differential equation, i.e. elliptic, parabolic and hyperbolic equations. No compatibility requirements need to be imposed between approximating function spaces for mixed problems. Furthermore, no stabilization is required for convection dominated flows.

When we use the Fictitious Domain approach together with LSqSEM, this leads to symmetric indefinite systems and compatibility requirements need to be imposed between approximating spaces of Lagrange multipliers, used to enforce the constraints on the immersed boundary, and the other functions. It may seem the introduction of Fictitious Domain approach sacrifices the benefits of least-squares formulation, but the peculiarities of LSqSEM are still advantageous for the coupled method, as illustrated in Section 4.

The above mentioned coupled methodology, the Fictitious Domain-Least Squares Spectral Element Method (FD-LSqSEM), have been already proposed by the authors in a previous work [29] for the solution of general two-dimensional elliptic problems. The aim of the present paper is its theoretical and numerical implementation for the solution of two-dimensional fluid dynamic incompressible equations.

The paper is organized as follows: Section 2 presents the concept of Fictitious Domain. Section 3 introduces the governing fluid dynamic equations and the formulation of Fictitious Domain method for Navier–Stokes flows. In Section 4 a brief summary of the Spectral Element Method is given. Section 5 considers different test problems. Good accuracy properties of the method are demonstrated by numerical experiments. These ones are performed with several mesh size and polynomial order of modal functions to better quantify the performance of the proposed solution procedure. In Section 6 all the results for the two-dimensional implementation of FD-LSqSEM will be discussed.

2. Fictitious Domain approach

Fictitious Domain approach have been developed for the solution of differential problems defined on domain changing in time and space, i.e. in general structural elastic problems, fluid dynamics problems with moving rigid bodies, shape optimization problems, differential equations defined on stochastic domain, and so on. This means the same problem is solved on different domains.

Unlike the usual approach, based on the boundary variation technique where a sequence of domains is considered (Fig. 1), according to Fictitious Domain approach (Fig. 2) the computational domain is not the same as the physical domain of the problem, but it contains that one. Hence when the physical domain changes the computational domain does not change with evident advantages.

Several variants of Fictitious Domain method exist: the basic idea is to extend the operator and the domain into a larger simple shaped domain. The most important ways to do this are algebraic and functional analytic approaches. In algebraic Fictitious Domain methods the problem is extended typically at the algebraic level in such a way that the solution of the original problem is obtained directly as a restriction of the solution of the extended problem without any additional constraint. There are several variants of such an approach [30] and they can be rather efficient, but typically they are restricted to quite a narrow class of problems. More flexibility and better efficiency can be obtained by using a functional analytic approach [21] where the use of constraints ensures that the solution of the extended problem coincides with the solution of the original problem.

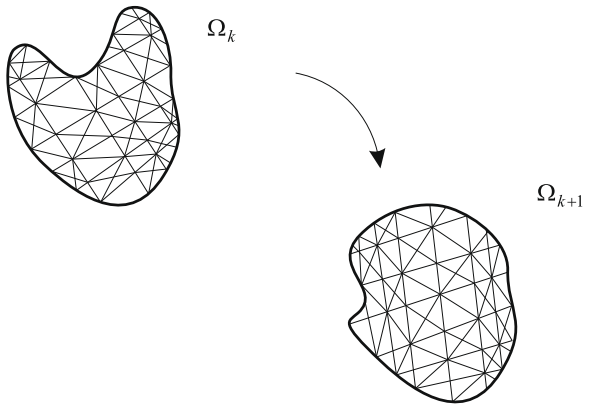

Fig. 1. Classical approach based on the boundary variation technique to solve differential problems defined on domain changing in time and space.

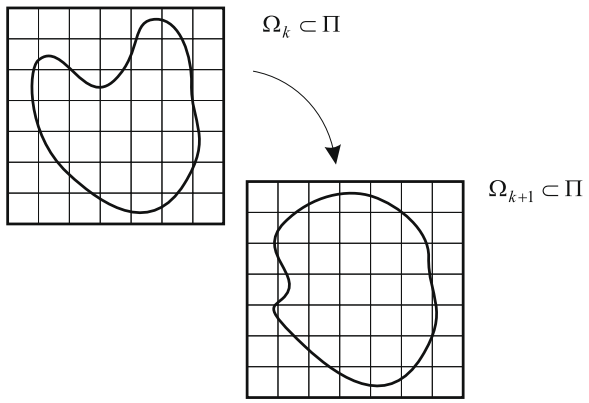

Fig. 2. Fictitious Domain approach to solve differential problems defined on domain changing in time and space.

In our implementation we enforce constraints by Lagrange multipliers [29].

The physical aspects of the problem can always be stated in a variational principle form, which specifies a scalar quantity, the functional J, defined by an integral form

$$J = \int_{\Omega} F\left(\phi, \frac{\partial \phi}{\partial x}, \frac{\partial \phi}{\partial y}, \ldots, x, y, \ldots\right) d\Omega + \int_{\Gamma} E\left(\phi, \frac{\partial \phi}{\partial x}, \frac{\partial \phi}{\partial y}, \ldots, x, y, \ldots\right) d\Gamma \tag{1}$$

where $\Gamma = \partial\Omega, \phi$ is the unknown function and F and E are specified operators. The solution to the continuum problem is a function ϕ which make J stationary with respect to small changes $\delta\phi$; thus, for a solution to the continuum problem, the variation is $\delta J = 0$.

To implement the Fictitious Domain approach we have to extend the operator F and the domain Ω into a larger simple shaped domain Π and to constrain the functional on $\Gamma = \partial\Omega$ (Fig. 3). To treat such problems Lagrangian multipliers are introduced, so that the problem is now equivalent to find the stationary point of J', where

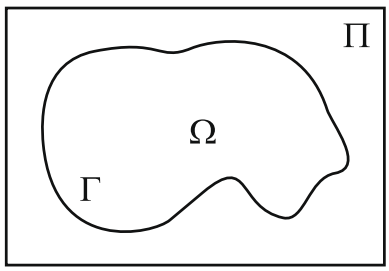

Fig. 3. Example of a fictitious rectangular domain Π containing the original domain Ω.

$$J' = \int_{\Pi} F\left(\phi, \frac{\partial\phi}{\partial x}, \frac{\partial\phi}{\partial y}, \ldots, x, y, \ldots\right) d\Omega + \int_{\Gamma} \lambda(\mathbf{x}) E\left(\phi, \frac{\partial\phi}{\partial x}, \frac{\partial\phi}{\partial y}, \ldots, x, y, \ldots\right) d\Gamma \tag{2}$$

Here $\lambda(\mathbf{x})$ is an undetermined multiplier which is in general a function of position, because the local condition must be satisfied at every point of Γ, rather than being a global restriction.

About the extension of the operator F to the fictitious region, different choices are possible. A common way is to set all the known functions that appear on the operator F to zero. Moreover in literature there are examples where homogeneous or periodic constraints are enforced on the boundary $\Gamma_{\Pi} = \partial\Pi$ of fictitious domain. By our experience all these choices influence the accuracy of the numerical solution, in particular in the region close to the immersed boundary. In our opinion the best way is to extend the operator F in banal way, that is it will be defined as in the domain Ω, and to not enforce additional constraints on the boundary of the fictitious domain.

3. The incompressible Navier–Stokes equations

3.1. The stationary Navier–Stokes equations governing incompressible flow

We consider the stationary Navier–Stokes equations governing incompressible flow, which in dimensionless form can be stated as follows:

$$(\mathbf{u}\cdot\nabla)\mathbf{u} + \nabla p + \frac{1}{Re}\nabla\cdot[(\nabla\mathbf{u}) + (\nabla\mathbf{u})^T] = \mathbf{f} \quad \text{in } \Omega \tag{3}$$

$$\nabla\cdot\mathbf{u} = 0 \quad \text{in } \Omega \tag{4}$$

$$\mathbf{u} = \mathbf{u}^s \quad \text{on } \Gamma_u \tag{5}$$

$$\boldsymbol{\sigma}\cdot\hat{\mathbf{n}} = \mathbf{f}^s \quad \text{on } \Gamma_f \tag{6}$$

where $\Gamma = \partial\Omega = \Gamma_u \cup \Gamma_f$ and $\Gamma_u \cap \Gamma_f = \emptyset$, Re is the Reynolds number, $\mathbf{u}$ is the velocity vector, p is the pressure, $\mathbf{f}$ is a dimensionless force, $\boldsymbol{\sigma} = -p\mathbf{I} + 1/Re[(\nabla\mathbf{u}) + (\nabla\mathbf{u})^T]$, $\hat{\mathbf{n}}$ is the outward unit normal on the boundary of Ω, $\mathbf{u}^s$ is the prescribed velocity on the boundary Γ_u and $\mathbf{f}^s$ are the prescribed tractions on the boundary Γ_f. We assume that the problem is well posed and that a unique solution exists.

3.2. The vorticity based first-order system

We proceed replacing the problem with its first-order equivalent system. We introduce the vorticity vector, $\boldsymbol{\omega} = \nabla\times\mathbf{u}$, then by making use of the vector identity

$$\nabla\times\nabla\times\mathbf{u} = -\nabla^2\mathbf{u} + \nabla(\nabla\cdot\mathbf{u}) \tag{7}$$

and in view of the incompressibility constraint given in Eq. (4), the stationary Navier–Stokes equations can be written as follows:

Find the velocity $\mathbf{u}(\mathbf{x})$, pressure $p(\mathbf{x})$ and vorticity $\boldsymbol{\omega}(\mathbf{x})$ such that

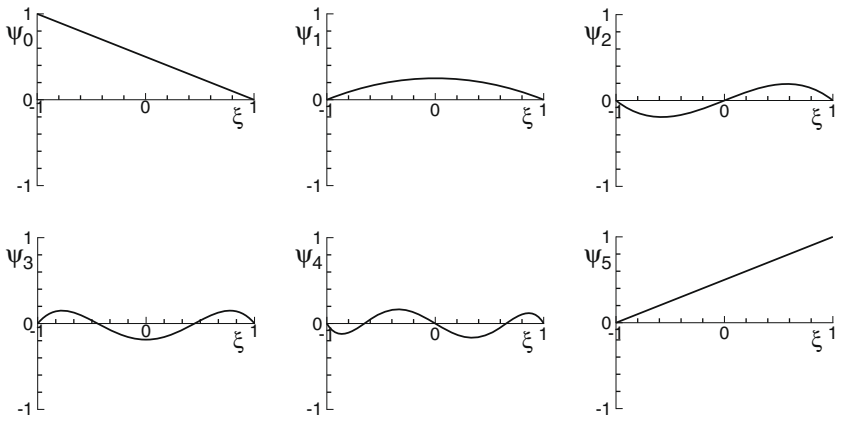

Fig. 4. Shape of modal expansion modes for the polynomial order $P = 5$.

$$(\mathbf{u}\cdot\nabla)\mathbf{u}+\nabla p+\frac{1}{Re}\nabla\times\boldsymbol{\omega}=\mathbf{f}\quad\text{in }\Omega \tag{8}$$

$$\boldsymbol{\omega}-\nabla\times\mathbf{u}=\mathbf{0}\quad\text{in }\Omega \tag{9}$$

$$\nabla\cdot\mathbf{u}=0\quad\text{in }\Omega \tag{10}$$

$$\nabla\cdot\boldsymbol{\omega}=0\quad\text{in }\Omega \tag{11}$$

$$\mathbf{u}=\mathbf{u}^s\quad\text{on }\Gamma_u \tag{12}$$

$$\boldsymbol{\omega}=\boldsymbol{\omega}^s\quad\text{on }\Gamma_\omega \tag{13}$$

The seemingly redundant Eq. (11) is needed in the three-dimensional case to make the system of equations uniformly elliptic [31]. Typically $\Gamma_u\cap\Gamma_\omega=\emptyset$, i.e. if velocity is specified at a boundary, vorticity does not need to be specified there.

3.3. Fictitious domain formulation for Navier–Stokes equations

Let be Π the fictitious domain including Ω. We define the Lagrangian $L:\mathbf{X}\times M\to\Re$ as follows:

$$\begin{aligned}L(\mathbf{u},p,\boldsymbol{\omega},\lambda;\mathbf{f})=&\frac{1}{2}\left(\left\|(\mathbf{u}\cdot\nabla)\mathbf{u}+\nabla p+\frac{1}{Re}\nabla\times\boldsymbol{\omega}-\mathbf{f}\right\|^2_{0,\Pi}+\|\boldsymbol{\omega}-\nabla\times\mathbf{u}\|^2_{0,\Pi}+\|\nabla\cdot\mathbf{u}\|^2_{0,\Pi}+\|\nabla\cdot\boldsymbol{\omega}\|^2_{0,\Pi}\right)+\langle\lambda,\tau\mathbf{u}\rangle_{0,\Gamma_u}\\&-\langle\lambda,\mathbf{u}^s\rangle_{0,\Gamma_u}+\langle\lambda,\tau\boldsymbol{\sigma}\cdot\hat{\mathbf{n}}\rangle_{0,\Gamma_f}-\langle\lambda,\mathbf{f}^s\rangle_{0,\Gamma_f}\end{aligned} \tag{14}$$

with $\mathbf{X}=\{(\mathbf{u},p,\boldsymbol{\omega})\in\mathbf{H}^1(\Pi)\times H^1(\Pi)\times\mathbf{H}^1(\Pi)\}$ and $M=\{\lambda\in H^{-1/2}(\Gamma)\}$, where the Lagrange multiplier defined on Γ is denoted by λ, $\langle\cdot,\cdot\rangle$ is the duality pairing between $M:=H^{-1/2}(\Gamma)$ and $H^{1/2}(\Gamma)$ and $\tau:H^1(\Pi)\to H^{1/2}(\Gamma)$ is the trace mapping.

If constraints have to be enforced on the boundary of the fictitious domain (for example the flow past a body), the velocity and vorticity constraints will be imposed in strong way, the outflow boundary condition will be enforced in weak sense as suggested by Ref. [27] for the least-squares formulation.

Using standard calculus of variations techniques we obtain the saddle-point problem:

$$\begin{cases}\text{Find }(\mathbf{u},p,\boldsymbol{\omega},\lambda)\in\mathbf{X}\times M\text{ such that}\\ a((\mathbf{u},p,\boldsymbol{\omega}),(\mathbf{v},q,\boldsymbol{\psi}))+b((\mathbf{v},q,\boldsymbol{\psi}),\lambda)=l((\mathbf{v},q,\boldsymbol{\psi}))\quad\forall(\mathbf{v},q,\boldsymbol{\psi})\in\mathbf{X}\\ b((\mathbf{u},p,\boldsymbol{\omega}),\mu)=g(\mu)\quad\forall\mu\in M\end{cases} \tag{15}$$

where

$$\begin{aligned}a((\mathbf{u},p,\boldsymbol{\omega}),(\mathbf{v},q,\boldsymbol{\psi}))=&\int_\Pi\left((\mathbf{u}\cdot\nabla)\mathbf{u}+\nabla p+\frac{1}{Re}\nabla\times\boldsymbol{\omega}\right)\left((\mathbf{v}\cdot\nabla)\mathbf{v}+\nabla q+\frac{1}{Re}\nabla\times\boldsymbol{\psi}\right)d\pi\\&+\int_\Pi(\boldsymbol{\omega}-\nabla\times\mathbf{u})\cdot(\boldsymbol{\psi}-\nabla\times\mathbf{v})d\pi+\int_\Pi(\nabla\cdot\mathbf{u})\cdot(\nabla\cdot\mathbf{v})d\pi+\int_\Pi(\nabla\cdot\boldsymbol{\omega})\cdot(\nabla\cdot\boldsymbol{\psi})d\pi\end{aligned} \tag{16}$$

$$b((\mathbf{u},p,\boldsymbol{\omega}),\mu)=\int_{\Gamma_u}\mathbf{u}\mu d\gamma+\int_{\Gamma_f}(\boldsymbol{\sigma}\cdot\hat{\mathbf{n}})\mu d\gamma \tag{17}$$

$$l((\mathbf{v},q,\boldsymbol{\psi}))=\int_\Pi\mathbf{f}\cdot\left((\mathbf{v}\cdot\nabla)\mathbf{v}+\nabla q+\frac{1}{Re}\nabla\times\boldsymbol{\psi}\right)d\pi \tag{18}$$

$$g(\mu)=\int_{\Gamma_u}\mathbf{u}^s\mu d\gamma+\int_{\Gamma_f}\mathbf{f}^s\mu d\gamma. \tag{19}$$

The solution of the original problem, Eqs. (3)–(6), will be the restriction to Ω of the extremum of Lagrangian Eq. (14).

Following the procedure outlined in Section 4 we discretized the saddle-point problem Eq. (15) and we generate a system of equations for the modal unknown coefficients associated with velocity, pressure, vorticity and Lagrange multipliers. Once the discrete problem is obtained, it is linearized by Newton's method [32].

4. *hp*-Finite element approximation

To get the approximate solution of the minimization problem of least squares functional a numerical method has to be used. The spectral *hp* element method is a numerical technique for solving partial differential equations based on the variational formulation of boundary and initial value problems [33–36]. The solution is represented by a finite number of basis functions. The spectral *hp* element method is based on higher-order functions, which are locally defined over finite size parts of domain (elements). The advantage of such kind of method with respect to traditional finite element method is its exponential convergence property with the increasing of polynomial order p, if the exact solution is sufficiently smooth.

Historically there is a distinction between *hp* type FEM and spectral element method due to the expansion which can be modal or nodal. In *hp*-FEM the expansion basis is usually modal, i.e. the basis functions are of increasing order (hierarchical) and the set of order $p-1$ is contained within the set of order p. In modal approach the expansion coefficients do not have any

particular physical meaning. In contrast in nodal spectral element method the expansion basis are non-hierarchical and consists of $p+1$ polynomial of order p. Moreover the expansion coefficients are associated with a set of nodal points where only one basis function has non-zero value. Hence the expansion coefficients can be interpreted as the physical solution values at the nodal points. The methods are mathematically equivalent, in numerical practice, however the two approaches do have different numerical properties in terms of implementation efficiency, ability to vary the polynomial order and conditioning of global sparse systems (see Ref. [33] for more details). In our implementation we choose a modal approach.

We proceed to define a discrete problem by choosing appropriate finite element subspaces for the unknown functions $\mathbf{u}$, p and $\boldsymbol{\omega}$ and the Lagrange multiplier λ.

There are no restrictive compatibility conditions on the discrete spaces of $\mathbf{u}$, p and $\boldsymbol{\omega}$, so we choose the same finite element subspace for each of the variables. The only requirement for approximating spaces is that we choose continuous piecewise polynomials that are at least bi-linear in two dimensions or tri-linear in three dimensions.

Consider the two-dimensional case and let $\mathscr{P}_h$ be a family of quadrilateral finite elements $\overline{\Pi}_e$ that make up the connected model $\overline{\Pi}_h$. We map $\overline{\Pi}_e$ to a bi-unit square $\widehat{\Pi}_e = [-1,1]\times[-1,1]$, where (ξ,η) is a point in $\widehat{\Pi}_e$. In general, over a typical element $\widehat{\Pi}_e$, we approximate the scalar function ϕ by the expression

$$\phi(\xi,\eta) = \sum_{i=1}^{n} \tilde{\phi}_i \varphi_i(\xi,\eta) \quad \text{in } \widehat{\Pi}_e \tag{20}$$

In modal expansion, φ_i are tensor products of the one-dimensional C^0 p-type hierarchical basis

$$\psi_p = \begin{cases} \frac{1-\xi}{2} & \text{for } p = 0 \\ \frac{1-\xi}{2}\frac{1+\xi}{2}P_{p-1}^{\alpha,\beta} & \text{for } 0 < p < P,\ P \geqslant 1 \\ \frac{1+\xi}{2} & \text{for } p = P \end{cases} \tag{21}$$

shown in Fig. 4 for $P = 5$, and $\tilde{\phi}_i$ are coefficients associated with each of the modes of hierarchical basis. In Eq. (21) $P_p^{\alpha,\beta}$ are the Jacobi polynomials [37] of order p, in particular ultraspheric polynomials corresponding to the choice $\alpha = \beta$ with $\alpha = \beta = 1$. This choice is due to the considerations about the sparsity of the matrices we obtain discretizing the problem presented by Ref. [33]. In Fig. 5 we show the construction of a two-dimensional modal expansion basis from the product of two one-dimensional expansions of order $P = 4$.

In the saddle-point problem Eq. (15) we approximate the components of the vector valued functions $\mathbf{u}$ and $\boldsymbol{\omega}$ and the scalar function p by Eq. (20).

The approximation of Lagrange multipliers requires the discretization of the immersed boundary Γ into curvilinear one-dimensional elements $\overline{\Gamma}_e$, which are mapped to linear unit elements $\widehat{\Gamma}_e = [-1,1]$. On these elements the function λ is approximated by the expression

$$\lambda(\xi) = \sum_{i=1}^{r} \tilde{\lambda}_i \psi_i(\xi) \quad \text{on } \widehat{\Gamma}_e \tag{22}$$

where ψ_i are defined in Eq. (21) and $\tilde{\lambda}_i$ are the coefficients associated with expansion modes of function λ.

The choice of Lagrange multipliers discrete space is not independent of the discrete spaces of variables $\mathbf{u}$, p and $\boldsymbol{\omega}$. To ensure the convergence of the solution of discretized model to that one of the continuous problem, the Ladyzhenskaja–Babuska–Brezzi (*LBB*)-condition, also known as inf-sup condition, has to be satisfied [38,39]:

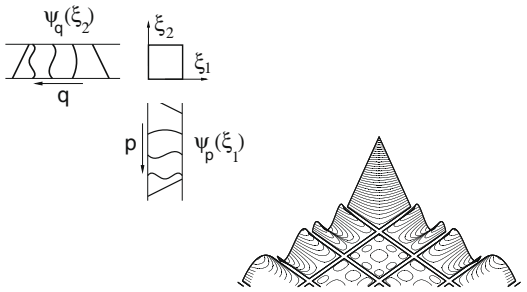

$$\sup_{\phi\in H^1(\Pi)} \frac{\int_\Gamma \mu\phi\, ds}{\|\phi\|_{H^1(\Pi)}} \geqslant \bar{\beta}\|\mu\|_{H^{-1/2}(\Gamma)}, \quad \forall \mu \in H^{-1/2}(\Gamma) \tag{23}$$

for some $\bar{\beta} > 0$ independent of the discretization.

In Ref.[12] it has been observed the Eq. (23) constraints the choice of H and h, where H is the characteristic length of Lagrange multiplier elements and h of fictitious domain elements. Intuitively one might think that the smaller the mesh size for the Lagrange multipliers is chosen, the more accurately one can enforce the boundary constraints. But it has been demonstrated the *LBB*-condition is satisfied whenever $H/h \geqslant c$, with c sufficiently large constant which depends on the domain in a complicated way. This says that the mesh size on the boundary should be larger than that on the domain.

The validity of the LBB condition has been the object of several investigations. In all these contributions the spaces of fictitious domain and Lagrange multipliers consist only of piecewise linear and piecewise constant functions, respectively. In this case, it has been shown that for $c = 3$, the LBB condition is satisfied (see Ref. [40]). In this work, where spectral element method is used, the satisfaction of Eq. (23) does not depend only on H and h, but on the chosen expansion polynomial order of the elements, too. In general the expansion polynomial order of the Lagrange multipliers will be lower than the expansion polynomial order of fictitious domain. The difference between the polynomial orders to be used depends on the ratio H/h. An example is shown in Section 5.1.

Finally, it should be mentioned that the obstructions caused by the LBB condition can be avoided by means of stabilization techniques, proposed in Ref. [41] and Ref. [42]. These methodologies are under study, for the improvement of the proposed algorithm.

Once the discrete spaces of the unknown functions have been chosen and the approximation is introduced in Eq. (15), we proceed to generate a system of linear algebraic equations at element level. The integrals in these equations are evaluated using Gauss–Legendre quadrature rules. The global system of equations is assembled from the element contributions using the direct summation approach.

The FD-LSqSEM produces symmetric indefinite matrices, but the assembled system of equations can be written as

$$\begin{pmatrix} \mathbf{A} & \mathbf{B}^T \\ \mathbf{B} & \mathbf{0} \end{pmatrix} \begin{pmatrix} \mathbf{\Phi} \\ \boldsymbol{\lambda} \end{pmatrix} = \begin{pmatrix} \mathbf{f} \\ \mathbf{g} \end{pmatrix} \tag{24}$$

where $\mathbf{A}$ is symmetric positive definite and $\mathbf{B}$ is the matrix coupling the primal variables $\mathbf{\Phi} = (\mathbf{u} \quad p \quad \omega)^T$ and the Lagrange multipliers $\boldsymbol{\lambda}$.

Let us remark the information on the geometry Ω is just in $\mathbf{B}$ and $\mathbf{g}$. From the first equation we know:

$$\mathbf{\Phi} = \mathbf{A}^{-1}(-\mathbf{B}^T\boldsymbol{\lambda} + \mathbf{f}), \tag{25}$$

so, being from the second equation $\mathbf{B\Phi} = \mathbf{g}$, we can write:

$$\mathbf{B}\mathbf{A}^{-1}\mathbf{B}^T\boldsymbol{\lambda} = \mathbf{B}\mathbf{A}^{-1}\mathbf{f} - \mathbf{g}. \tag{26}$$

We can solve this system by CG method. The size of $\mathbf{B}\mathbf{A}^{-1}\mathbf{B}^T$ is much smaller than the size of $\mathbf{A}$.

The advantage of using FD-LSqSEM is evident for problems with moving boundaries or if the same problem has to be solved for several different boundary conditions. For linear problems the matrix $\mathbf{A}$ remains unchanged, so the inversion of $\mathbf{A}$ has to be performed just once. A modification of Γ only affects $\mathbf{B}$ and $\mathbf{g}$, but not $\mathbf{A}$. Anyway the remeshing of Π is not necessary.

5. Numerical results and discussion

5.1. Flow past a 2D spinning cylinder near a moving wall

Let us consider the Wannier flow [33], which has an exact solution in the Stokes regime. The advantage to study a Stokes flow as first test case is the non-linear terms are not present in the governing equations, so there is no need for linearization methods.

The Wannier flow is the two-dimensional Stokes flow past a circular cylinder spinning counter-clockwise near a wall that moves in the streamwise direction. The exact solution (Appendix A) depends only on cylinder radius, R, its rate of rotation, ω, the distance between the center of the cylinder to the moving wall, d, and the velocity of the wall, U (see Fig. 6).

The parameters are chosen as $U = 1.0,\ \omega = 2.0,\ R = 0.25$ and $d = 0.75$. In the simulation Dirichlet boundary conditions are applied in each direction and the pressure $p = 0$ is enforced in the up-right corner. Fig. 7 shows the contours of u and v velocity components of the exact solution.

In order to analyze the behavior of LSqSEM when a Fictitious Domain approach is used, we investigate the p-convergence rates with fixed h-type discretization of fictitious domain and fixed hp-discretization of immersed boundary.

The fictitious domain we use is $\overline{\Pi} = [-0.75, 0.75] \times [-0.75, 0.75]$ including Ω. To test the FD-LSqSEM approach we consider the connected model Π^h of the computational domain Π shown in Fig. 8(a).

We use the modal expansions, i.e. the Legendre polynomials, both for quadrilateral elements of fictitious domain and for curvilinear elements of immersed boundary. The resulting linear system of equations is solved using a direct method, which

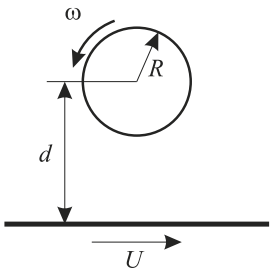

Fig. 6. Sketch of the flow past a spinning cylinder near a moving wall.

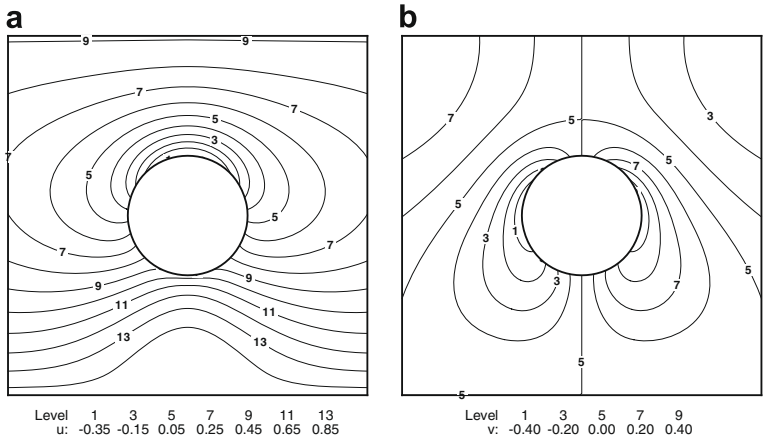

Fig. 7. Numerical solution of Wannier flow: (a) u-velocity contours and (b) v-velocity contours. The computational domain is shown in Fig. 8(a). The solution is obtained with expansion order of fictitious domain elements $P = 10$ and expansion order of immersed boundary elements $P = 5$.

performs an LU decomposition with partial pivoting and solves the triangular system through forward and backward substitution.

In Fig. 8, the Root Mean Square Errors (*RMSE*s) of u and v velocities are plotted as function of the expansion order p of fictitious domain in a linear–logarithmic scale. Each curve relates to a different p-level of the element approximation functions of the Lagrange multipliers on the immersed boundary Γ.

It is important to observe that the accuracy is pretty much the same for the variables u and v.

Spectral convergence of errors, typical of the LSqSEM case, is no more evident The behavior of FD-LSqSEM approach is due to *LBB*-condition. When the *hp*-refinement of immersed boundary is fixed, the *LBB*-condition is not satisfied for every *hp*-discretization of fictitious domain. But as long as the *LBB*-condition is satisfied the curves show a spectral convergence as in the LSqSEM case. This implies there is a relationship between the *hp*-discretization of the fictitious domain and *hp*-discretization of the immersed boundary which has to be satisfied for the spectral convergence of the method.

In general it has been observed that the difference between the polynomial orders to be used depends on the ratio H/h, where H is the characteristic length of Lagrange multiplier elements and h of fictitious domain elements. If the expansion polynomial order of the fictitious domain is P, the expansion polynomial order of the Lagrange multipliers should be $P-1$ for $H/h \approx 3, P-5$ for $H/h \approx 1$ and $P-9$ for $H/h \approx 1/3$. Figs. 9–11 show the *RMSE*s of u velocity as function of the expansion order P of fictitious domain in a linear–logarithmic scale, where each curve corresponds to a different constant difference between the polynomial orders of the fictitious domain and the Lagrange multipliers. Fig. 9 refers to a computational domain with $H/h \approx 3$, for $p - p_{LM} = 1$ a spectral convergence of the error can be observed. Fig. 10 refers to a computational domain with $H/h \approx 1$, for $p - p_{LM} = 5$ a spectral convergence of the error can be observed. Fig. 11 refers to a computational domain with $H/h \approx 1/3$, for $p - p_{LM} = 9$ a spectral convergence of the error can be observed.

Actually this behavior has been observed in most of the problems under study, but more tests and verifications are needed to assert this is a general rule.

5.2. Kovasznay flow

Let us consider a two-dimensional steady flow in $\overline{\Omega} = [-0.5, 1.5] \times [-0.5, 1.5]$. We use Kovasznay's solution (Appendix B) to the stationary incompressible Navier–Stokes equations to verify spectral convergence of the FD-LSqSEM numerical algorithm. Fig. 12 shows the exact solution for $Re = 40$, in particular the u-velocity field and the pressure field.

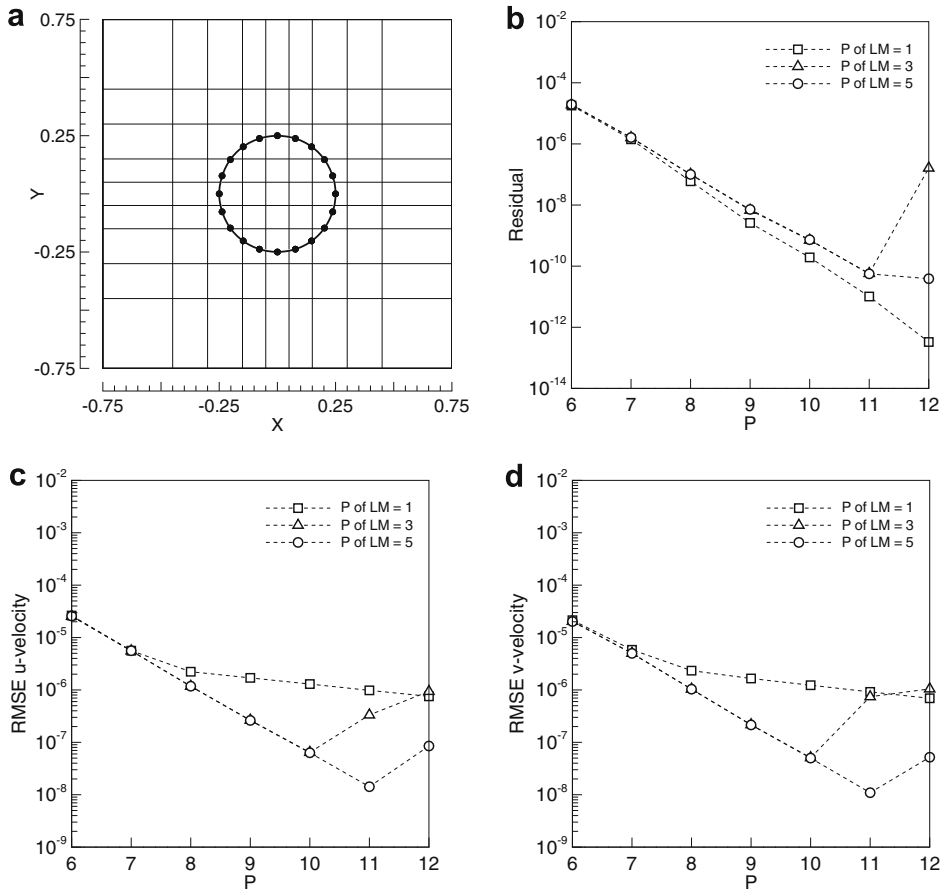

Fig. 8. Wannier flow: (a) computational domain using 81 quadrilateral elements and 20 immersed elements, (b) residual, (c) *RMSE* of u-velocity, (d) *RMSE* of v-velocity. The residual and the *RMSE* are plotted versus the expansion order P of fictitious domain elements. Several discretization p of Lagrange multipliers have been considered: Lagrange multiplier function has been expanded into a polynomial series of order $P = 1,\ P = 3$ and $P = 5$.

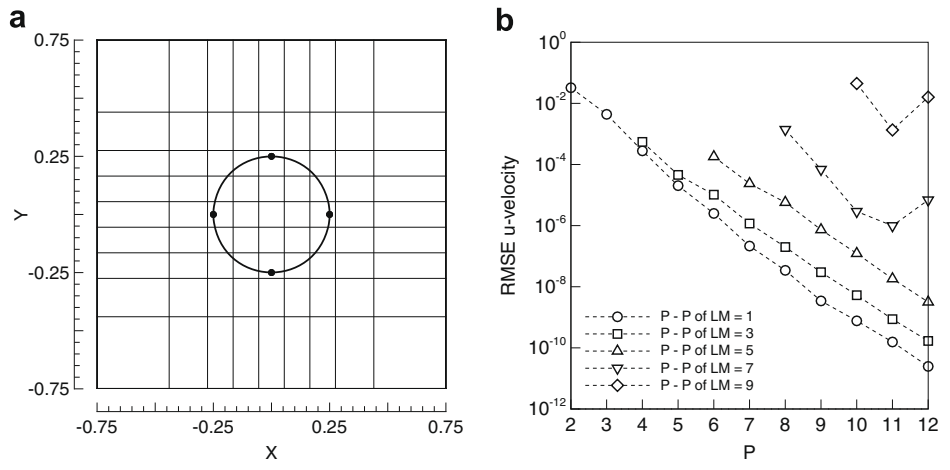

Fig. 9. Wannier flow: (a) computational domain with $H/h \approx 3$, (b) *RMSE* of u-velocity versus the expansion order P of the fictitious domain elements.

The fictitious domain we use is $\overline{\Pi} = [-0.75, 1.75] \times [-0.75, 1.75]$ including Ω. Fig. 13 shows the discretization of the domain into a non-uniform mesh of eight quadrilateral finite elements $\overline{\Pi}_e$. The exact solution is used to prescribe Dirichlet velocity boundary conditions on Γ and pressure is specified at point $(-0.5, -0.5)$. The immersed boundary Γ is discretized into linear elements. Several h-refinements are considered. Fig. 13 shows those ones investigated.

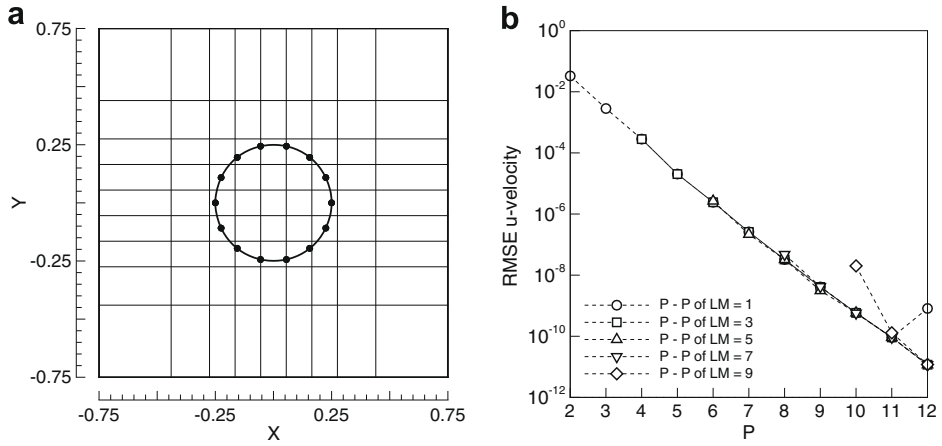

Fig. 10. Wannier flow: (a) computational domain with $H/h \approx 1$, (b) *RMSE* of u-velocity versus the expansion order P of the fictitious domain elements.

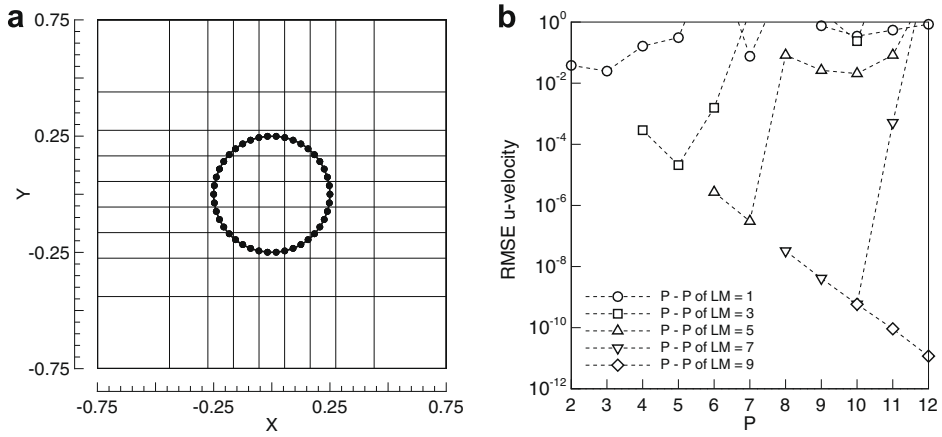

Fig. 11. Wannier flow: (a) computational domain with $H/h \approx 1/3$, (b) *RMSE* of u-velocity versus the expansion order P of the fictitious domain elements.

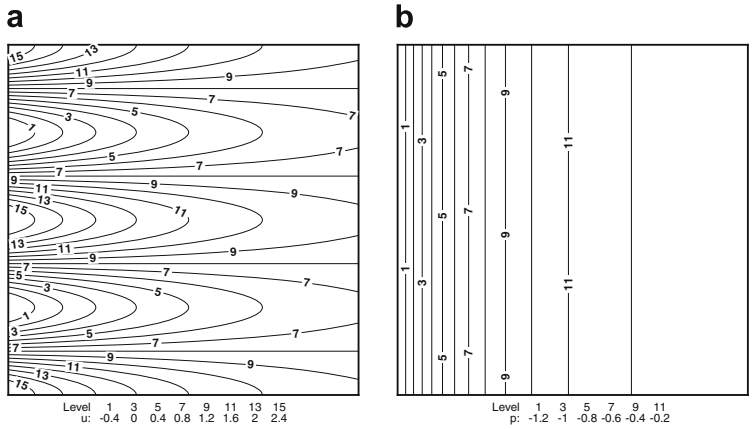

Fig. 12. Numerical solution of Kovasznay flow for $Re = 40$: (a) u-velocity contours and (b) pressure contours. The computational domain is shown in Fig. 13(a). The solution is obtained with expansion order of fictitious domain elements $P = 10$ and expansion order of immersed boundary elements $P = 5$.

The global system of equations we obtain assembling the element contributions is linearized using Newton's method and the resulting linear algebraic system of equations is solved using a direct algorithm based on LU decomposition at each New-

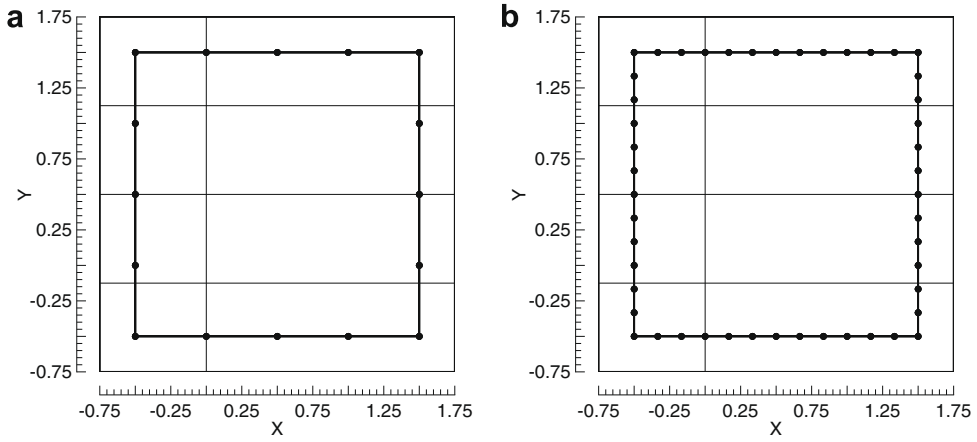

Fig. 13. Kovasznay flow: computational domains. The fictitious domain is discretized into eight quadrilateral finite elements. For the immersed boundary several *h*-refinements have been considered: (a) 16 immersed elements and (b) 48 immersed elements.

ton step. Non-linear convergence is declared when the relative norm of the residual in velocities $\|\Delta \mathbf{u}^{hp}\|/\|\mathbf{u}^{hp}\|$ is less than 10^{-4}.

In Figs. 14 and 15 we plot the Root Mean Square Error of the velocity u and pressure p fields as a function of the expansion order of the fictitious domain elements in a logarithmic–linear scale for the computational domain shown in Fig. 13(a) and Fig. 13(b), respectively.

Several discretization p of Lagrange multipliers are considered: Lagrange multipliers function are expanded into a polynomial series of order $p = 1$, $p = 3$ and $p = 5$. Moreover the error of numerical solution obtained by FD-LSqSEM is compared to the numerical solution obtained by LSqSEM using the non-uniform mesh of eight quadrilateral finite elements shown in Fig. 16.

Spectral convergence of errors, typical of the LSqSEM case, is evident. For the FD-LSqSEM approach we observe a different behavior due to *LBB*-condition and already described in the previous section.

It is important to observe that the computational domain used for the FD-LSqSEM solution and LSqSEM solution is discretized into eight quadrilateral spectral elements in both cases, but the computational domain used for the FD-LSqSEM solution is larger than the computational domain used for the LSqSEM solution. This explains why the errors of the LSqSEM solution is a few lower than those of FD-LSqSEM solution.

Fig. 17 shows the functional J for the computational domains shown in Fig. 13. These plots emphasize the behavior of FD-LSqSEM solution with increasing expansion order p of spectral elements due to *LBB*-condition.

5.3. Flow past a circular cylinder in a 2D channel

We next consider the two-dimensional flow of an incompressible fluid past a circular cylinder. The Reynolds numbers considered here are 20 and 40, for which a steady-state solution exists. The cylinder is of unit diameter and is placed in

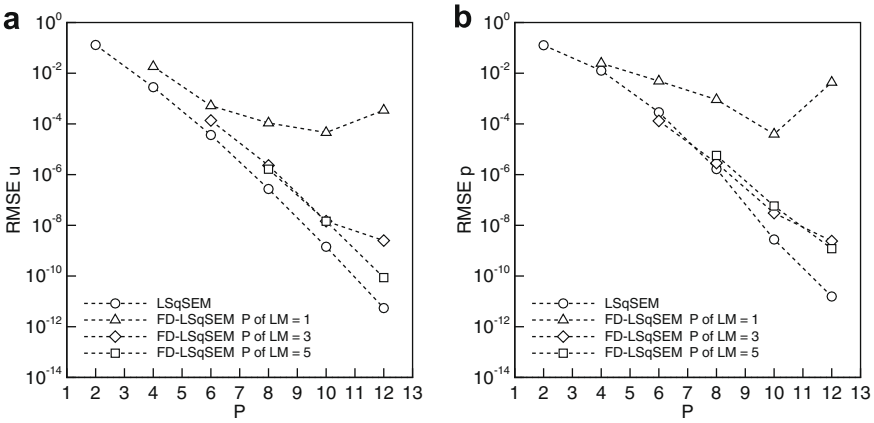

Fig. 14. Kovasznay flow: *RMSE* of numerical solution versus the expansion order P of fictitious domain elements for the computational domain shown in Fig. 13(a): (a) u-velocity and (b) pressure p. Several discretization p of Lagrange multipliers have been considered: Lagrange multipliers function has been expanded into a polynomial series of order $P = 1$, $P = 3$ and $P = 5$.

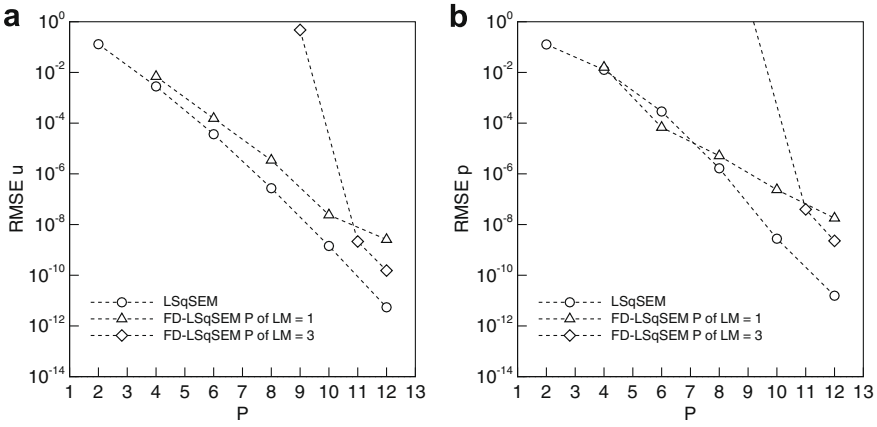

Fig. 15. Kovasznay flow: *RMSE* of numerical solution versus the expansion order P of fictitious domain elements for the computational domain shown in Fig. 13(b): (a) u-velocity and (b) pressure p. Several discretization p of Lagrange multipliers have been considered: Lagrange multipliers function has been expanded into a polynomial series of order $P = 1$ and $P = 3$.

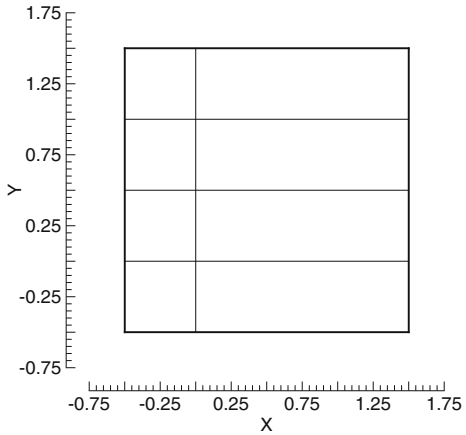

Fig. 16. Kovasznay flow: computational domain discretized into eight quadrilateral finite elements.

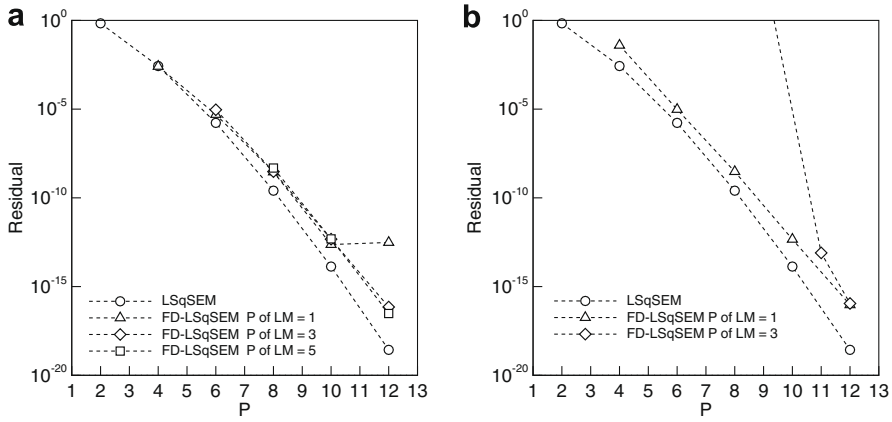

Fig. 17. Kovasznay flow: convergence of residual versus the expansion order P of fictitious domain elements (a) for the computational domain shown in Fig. 13(a) and (b) for the computational domain shown in Fig. 13(b). Several discretization p of Lagrange multipliers have been considered.

the finite region $[-15.5, 30.5] \times [-20.5, 20.5]$. The center of the cylinder lies at $(x, y) = (0, 0)$, so that the inflow is located 15.5 cylinder diameters in front of the center of the cylinder and the outflow boundary 30.5 cylinder diameters downstream of the center of the cylinder. The top and the bottom boundaries are located each 20.5 cylinder diameters above and below the center of the cylinder. The Reynolds number is based on the free-stream velocity and cylinder diameter.

The boundary condition imposed at the inflow, top and bottom boundaries is the free-stream velocity U_∞, specified to be unity, with y-component of velocity set to zero. The outflow boundary conditions are imposed in a weak sense through the least squares functional (see Ref. [27] for details).

The rectangular finite region $\overline{\Pi} = [-15.5, 30.5] \times [-20.5, 20.5]$ is the fictitious domain we consider. The connected model, Π^h, consists of 483 finite elements and is shown in Fig. 18. The immersed boundary Γ, where no-slip conditions are enforced, is discretized into twelve curvilinear finite elements. Fig. 19 shows a close-up view of the geometric discretization of fictitious domain around the circular cylinder and the discretization of the immersed boundary. We use a ninth-order modal expansion in each element of fictitious domain and a fourth-order modal expansion in each element of immersed boundary.

At each Newton step the linear system of equations is solved using a direct algorithm based on LU decomposition. Nonlinear convergence is declared when the relative norm of the residual in velocity between two consecutive iterations is less then 10^{-4}.

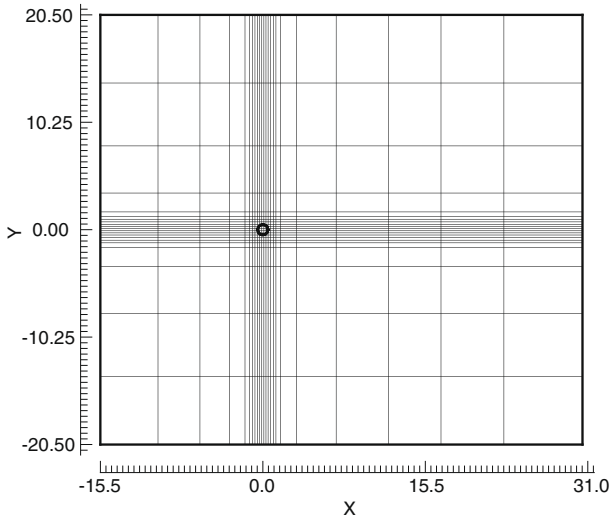

Fig. 18. Computational domain and mesh for flow past a circular cylinder: connected model.

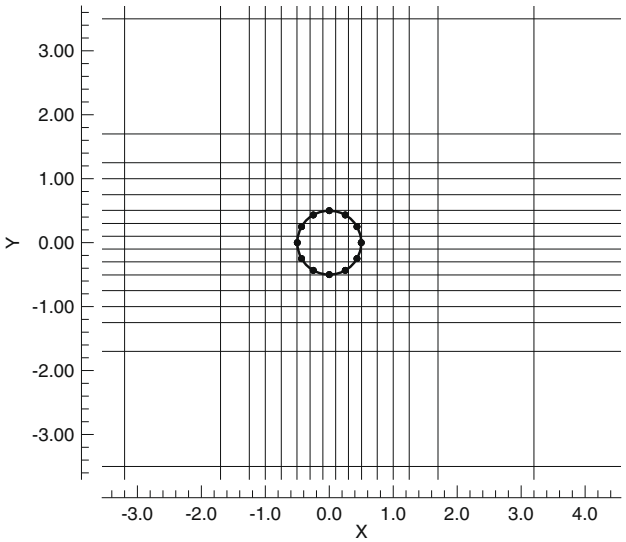

Fig. 19. Computational domain and mesh for flow past a circular cylinder: close-up view of the immersed boundary geometric discretization.

Fig. 20 shows the computed pressure coefficient distributions along the cylinder surface for $Re = 20$ and $Re = 40$, together with experimental measurements of Grove et al. [43] for the case $Re = 40$. We observe that the simulation result is in good agreement with the experimental measurements.

Figs. 21 and 22 show the pressure contours and the streamlines in the wake region for $Re = 20$ and $Re = 40$, respectively.

The computed drag coefficient for flow conditions of $Re = 20$ is $C_D = 2.0862$ and the predicted wake extends 0.9316 cylinder diameters measured from the back of the cylinder. For the case $Re = 40$ the computed drag coefficient is $C_D = 1.5525$ and the length of wake bubble is 2.2745 cylinder diameters.

The comparison of computed values of drag coefficient and wake length with those ones found in literature is really interesting. In Table 1 there is a collection of the values which can be found in previous works, both of experimental and numerical type. The values obtained by FD-LSqSEM with different expansion polynomial orders are also shown.

We can compute the mean and the standard deviation of the referenced data. For the case $Re = 20$ the mean value of C_D is 2.0365 and its standard deviation 0.0319, the mean value of wake length is 0.9225 and its standard deviation 0.0162. For the case $Re = 40$ the mean value of C_D is 1.5706 and its standard deviation 0.0696, the mean value of wake length is 2.2288 and its standard deviation 0.0870.

In Figs. 23 and 24 the diagrams of all collected values are shown. The mean value E and the confidence interval $E \pm \sigma$ are plotted too. Assuming that the data are from an approximately normally distributed population, about 68% of the values are within one standard deviation of the mean. It is worth to notice the values obtained by FD-LSqSEM always follow in the confidence interval, except for the drag coefficient with $Re = 40$ using a sixth-order modal expansion in the elements of fictitious domain. So we can see our solutions are in good agreement with both the experimental and numerical solutions found in

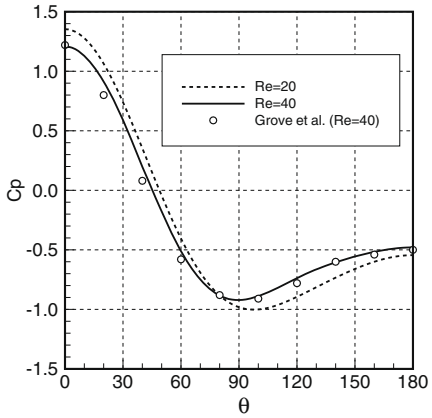

Fig. 20. Flow past a circular cylinder at $Re = 20$ and $Re = 40$: computed pressure coefficients distributions along the cylinder surface. Comparison with experimental measurements of Grove et al. [43] for the case $Re = 40$.

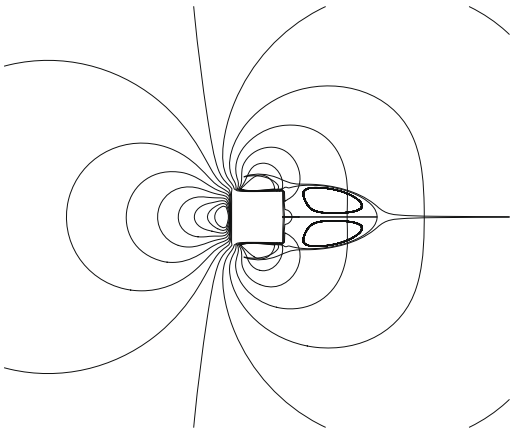

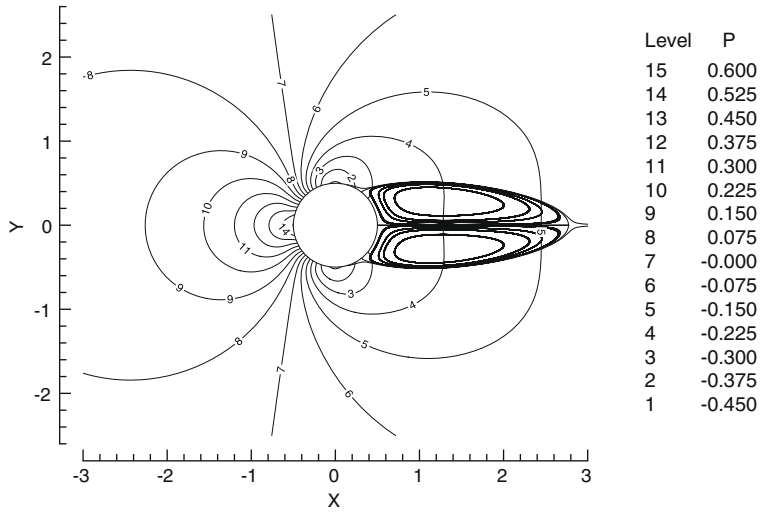

Fig. 22. Flow past a circular cylinder at $Re = 40$: pressure contours and streamlines in the wake region.

Table 1
Flow past a circular cylinder at $Re = 20$: drag coefficient C_D.

ID study	References	C_D $Re = 20$	C_D $Re = 40$	L_{sep} $Re = 20$	L_{sep} $Re = 40$
1	[44s]	2.0200	1.6500	–	–
2	[45]	2.0500	1.7000	–	–
3	[46]	2.0450	1.5220	0.94	2.345
4	[47]	2.0001	1.4980	0.91	2.24
5	[48]	2.0300	1.5200	0.92	2.27
6	[49]	2.0027	1.5359	0.935	2.325
7	[50]	2.0530	1.5500	0.893	2.1785
8	[51]	1.9980	1.4940	–	–
9	[52]	2.0800	1.5490	0.932	2.29
10	[53]	–	1.6750	0.90	2.10
11	[54]	–	1.6000	–	–
12	[27]	2.0862	1.5537	0.93	2.275
13	[55]	–	–	0.935	2.135
14	[56]	–	–	0.93	2.130
15	Present prediction	2.0862	1.5525	0.9316	2.2745

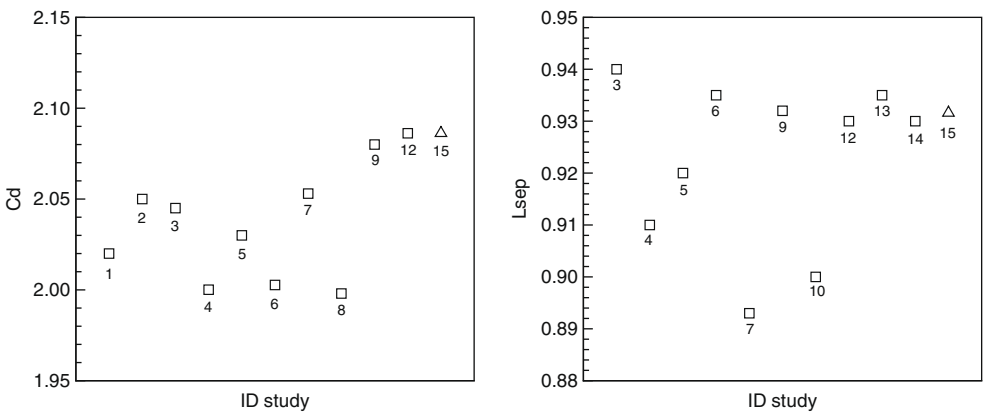

Fig. 23. Flow past a circular cylinder at $Re = 20$: drag coefficient C_D and length of wake bubble L_{sep}. The ID refers to Table 1.

literature. In particular we can observe that the solution we obtain with expansion polynomial order $p = 9$ of fictitious domain elements are really close to those ones obtained by Pontaza and Reddy by means of the LSqSEM in Ref. [27].

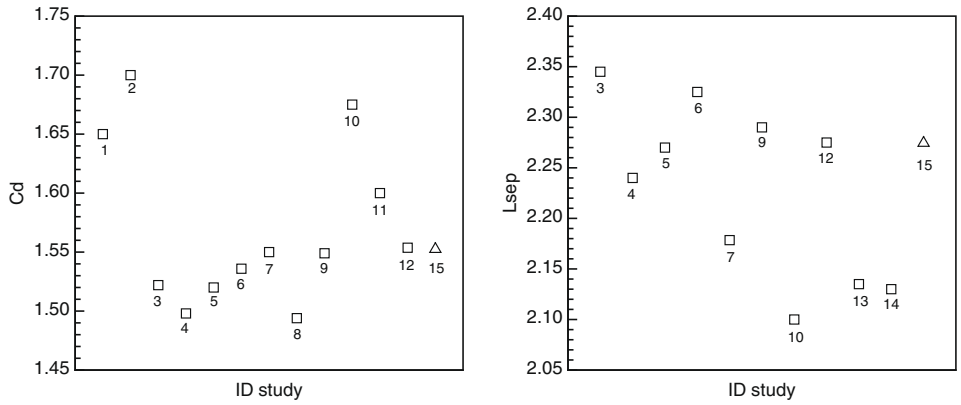

Fig. 24. Flow past a circular cylinder at $Re = 40$: drag coefficient C_D and length of wake bubble L_{sep}. The ID refers to Table 1.

5.4. Flow over a backward-facing step

We consider the two-dimensional steady flow over a backward-facing step at $Re = 800$. The two-dimensional flow past a backward-facing step is a standard test problem and it has been addressed by numerous authors using a variety of numerical and experimental methods [57–61].

The basic flow situation is shown in Fig. 25. Fluid flows with an average velocity U past a step of height H with channel heights upstream and downstream of the step represented by H_u and H_d, respectively. After the flow separates at the step, the flow reattaches to the lower wall at the distance x_r.

In this work the geometry and boundary conditions are taken from the solution of Lee and Mateescu [57]. The expansion ratio H_d/H_u tested is 2.0. The origin of the coordinate system is centered at the step corner. H_u is equal to 1.5 and L_u, the length of the upstream channel, is equal to 5.0. The total length of the channel L is 95.0. The flow is characterized by a Reynolds number $Re = UH_d/\nu$ where U is the average cross-section velocity and ν the kinematic viscosity.

We discretize the fictitious domain, $\overline{\Pi} = [-5.0, 90.0] \times [-1.5, 1.5]$ using 63 finite elements. The connected model, Π^h, is shown in Fig. 26. The immersed boundary Γ, where no-slip conditions are enforced, is discretized into four linear finite elements. We use an 11th-order modal expansion in each element of fictitious domain and a fifth-order modal expansion in each element of immersed boundary. The resulting discrete model is linearized using Newton's method. Non-linear convergence is declared when the relative norm of the residuals in velocities, $\|\Delta \mathbf{u}^{hp}\|/\|\mathbf{u}^{hp}\|$, is less than 10^{-4}. The analysis starts with $Re = 100$ and steps to $Re = 800$ using a solution continuation technique with increments of $Re = 100$.

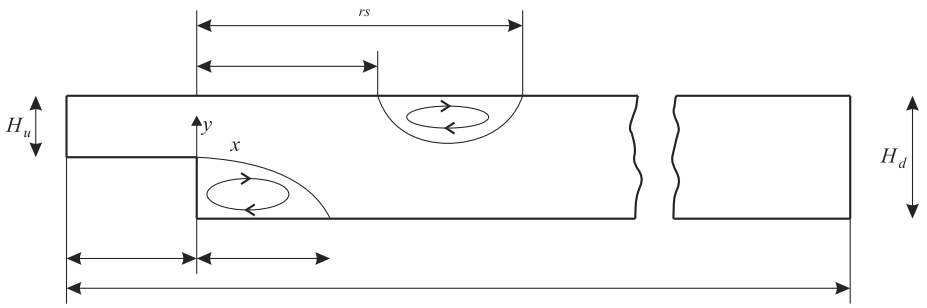

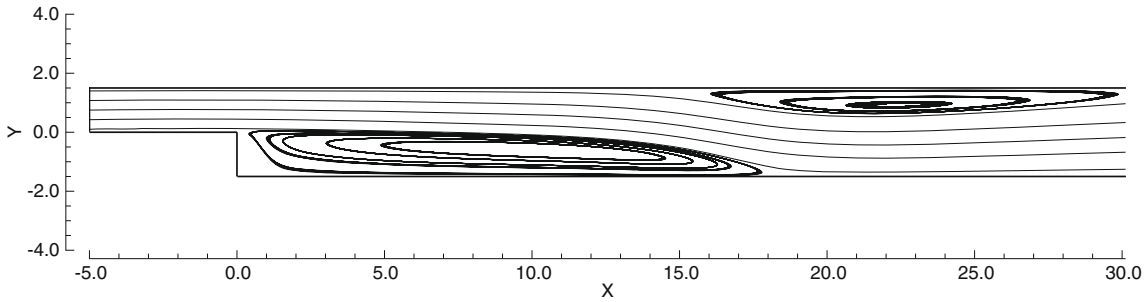

Fig. 27. Flow over a backward-facing step at $Re = 800$: streamlines.

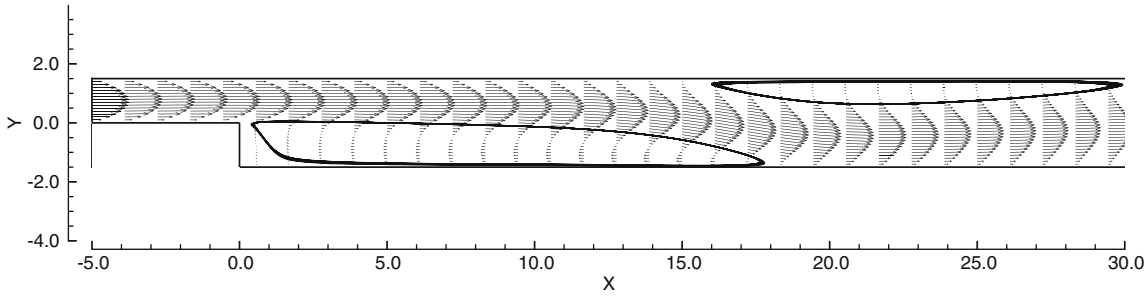

Fig. 28. Flow over a backward-facing step at $Re = 800$: vector velocity field.

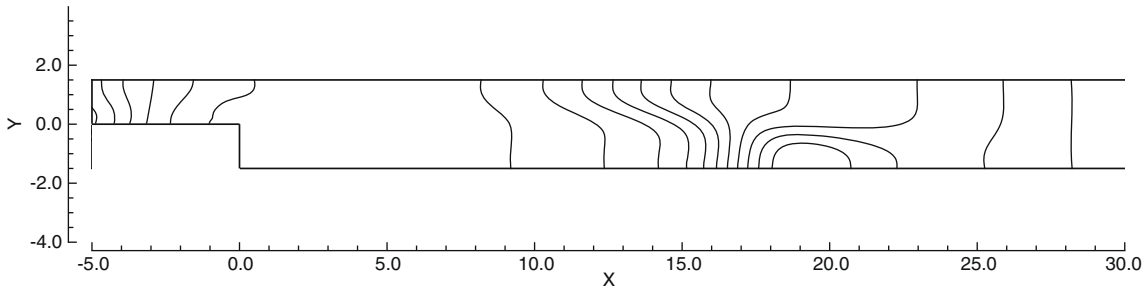

Fig. 29. Flow over a backward-facing step at $Re = 800$: pressure contours.

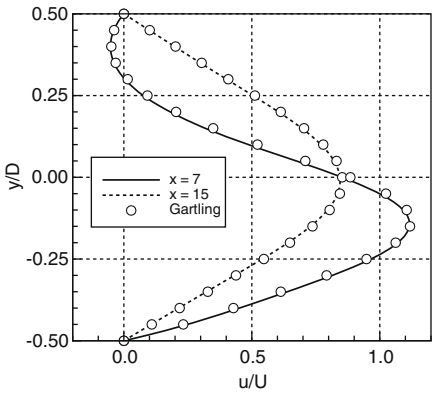

Fig. 30. Flow over a backward-facing step at $Re = 800$: horizontal velocity profiles along the height of the channel at $x/H_d = 7$ and $x/H_d = 15$. Comparison with the benchmark solution of Gartling [59].

Table 2
Flow over a backward-facing step at $Re = 800$: dimensionless length of reattachment on the lower wall x_r, dimensionless length of separation on the upper wall x_s and dimensionless length of reattachment on the upper wall x_{rs}.

ID study	References	x_r	x_s	x_{rs}
1	[57] (MHFS data)	6.45	5.15	10.25
2	[58]	–	5.70	10.00
3	[57]	6.0	4.80	10.30
4	[59]	6.1	4.85	10.48
5	[60]	6.0	–	–
6	[61]	5.8	–	–
7	Present prediction	6.00	5.08	10.35

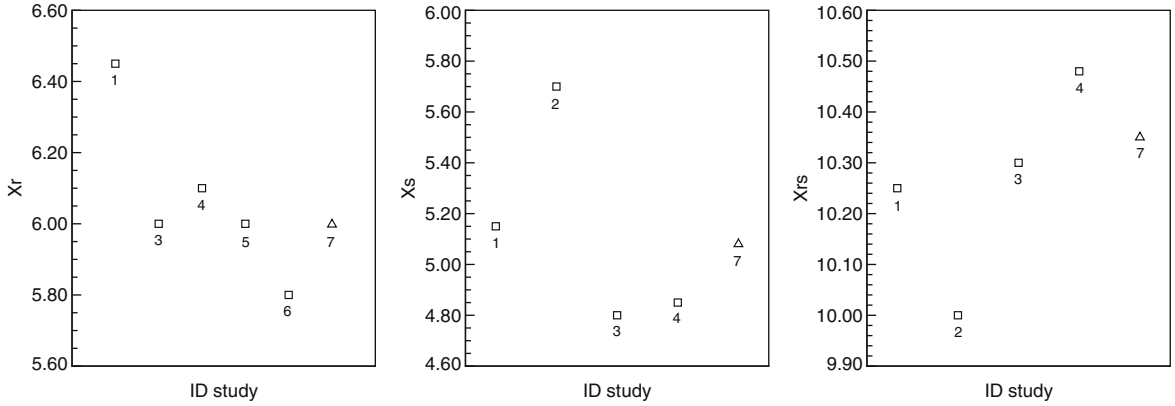

Fig. 31. Flow over a backward-facing step at $Re = 800$: dimensionless length of reattachment on the lower wall x_r, dimensionless length of separation on the upper wall x_s and dimensionless length of reattachment on the upper wall x_{rs}. The ID refers to Table 2.

Fig. 27 shows the streamlines of the computed solution, Fig. 28 the vector velocity field and Fig. 29 the pressure contours for $-5.0 \leqslant x \leqslant 30.0$, where the most of the interesting flow structures occur.

Fig. 30 shows the dimensionless velocity profiles, $u(y)/U$, along the channel height, y/H_d, at $x/H_d = 7$ and $x/H_d = 15$. We compare those ones with tabulated values from the benchmark solution of Gartling [59] and find excellent agreement.

Table 2 summarize the measurements of x_r, x_s and x_{rs} on the upper and lower walls for $Re = 800$ present in literature. We compare the results obtained in the present work with those found in literature.

Fig. 31 show diagrams of the measurements values found in literature with the values obtained by the FD-LSqSEM. Let us remark the values of x_r, x_s and x_{rs} computed in the present work are in good agreement with the referenced solutions.

6. Summary

In this paper we presented the formulation, validation and application of FD-LSqSEM for the Navier–Stokes equations.

The employed Fictitious Domain solver is based on Least Squares Spectral Element Method. This formulation is of particular interest to study problems on domain which changes in time and space, as Fictitious Domain approach allows avoiding the remeshing of computational domain in the presence of geometric variations. Its main advantage lies in the fact that only one Cartesian mesh, that represents the enclosure, needs to be generated.

The excellent convergence of the least squares functional and error were verified using the Wannier flow solution to the incompressible Stokes equations and the Kovasznay flow solution to the incompressible Navier–Stokes equations. The spectral convergence has been demonstrated till the *LBB*-condition is satisfied. Numerical results for steady flow past circular cylinder and incompressible flow over a backward-facing step were presented and found to be in excellent agreement with benchmark solutions.

Extension of the formulation to the non-stationary Navier–Stokes equations and compressible flows for subsonic/transonic flow conditions are the subject of forthcoming papers.

Acknowledgment

This work was partially supported by the project NODESIM-CFD *Non-Deterministic Simulation for CFD-based Design Methodologies* funded by the European Community represented by the CEC, Research Directorate-General, in the 6th Framework Programme, under Contract No. AST5-CT-2006-030959.

Appendix A. Wannier flow

The Wannier flow is the two-dimensional Stokes flow past a circular cylinder spinning counter-clockwise near a wall that moves in the streamwise direction. The exact solution of Wannier flow depends only on cylinder radius, R, its rate of rotation, ω, the distance between the center of the cylinder to the moving wall, d, and the velocity of the wall, U. If we place the origin of the coordinate system at the centre of the cylinder the exact solution is given by the following expressions:

$$u = U - 2(a_1 + a_0 Y_1)\left[\frac{s+Y_1}{K_1} + \frac{s-Y_1}{K_2}\right] - a_0 \ln\frac{K_1}{K_2} - \frac{a_2}{K_1}\left[s + Y_2 - \frac{(s+Y_1)^2 Y_2}{K_1}\right] - \frac{a_3}{K_2}\left[s - Y_2 - \frac{(s-Y_1)^2 Y_2}{K_2}\right] \tag{A.1}$$

$$v = \frac{2x}{K_1 K_2}(a_1 + a_0 Y_1)(K_2 - K_1) - \frac{x a_2 (s+Y_1) Y_2}{K_1^2} - \frac{x a_a (s-Y_1) Y_2}{K_2^2} \tag{A.2}$$

where

$$s = \sqrt{d^2 - R^2}, \quad \Gamma = \frac{d+s}{d-s}, \quad a_0 = \frac{U}{\ln \Gamma}, \quad a_1 = -d\left(a_0 + \frac{\omega R^2}{2s}\right)$$

$$a_2 = 2(d+s)\left(a_0 + \frac{\omega R^2}{2s}\right), \quad a_3 = 2(d-s)\left(a_0 + \frac{\omega R^2}{2s}\right)$$

$$Y_1 = y + d, \quad Y_2 = 2Y_1, \quad K_1 = x^2 + (s+Y_1)^2, \quad K_2 = x^2 + (s-Y_1)^2$$

Appendix B. Kovasznay flow

The solution of Kovasznay flow is given by

$$u = 1 - e^{\lambda x}\cos(2\pi y) \tag{B.1}$$

$$v = \frac{\lambda}{2\pi} e^{\lambda x}\sin(2\pi y) \tag{B.2}$$

$$p = p_0 - \frac{1}{2} e^{2\lambda x} \tag{B.3}$$

where $\lambda = Re/2 - (Re^2/4 + 4\pi^2)^{1/2}$ and p_0 is a reference pressure (an arbitrary constant).

References

[1] L. Parussini, V. Pediroda, Fictitious domain with least-squares spectral element method to explore geometric uncertainties by non-intrusive polynomial chaos method, CMES 22 (1) (2007) 41–64.
[2] L. Parussini, V. Pediroda, Investigation of multi geometric uncertainties by different polynomial chaos methodologies using a fictitious domain solver, CMES 23 (1) (2008) 29–52.
[3] V.K. Saul'ev, Solution of certain boundary-value problems on high-speed computers by the fictitious-domain method, Sibirsk. Mat. Z. 4 (1963) 912–925.
[4] E. Heikkola, Y.A. Kuznetsov, K. Lipnikov, Fictitious domain methods for the numerical solution of three-dimensional acoustic scattering problems, J. Comput. Acoust. 7 (1999) 161–183.
[5] U. Hetmaniuk, C. Farhat, A fictitious domain decomposition method for the solution of partially axisymmetric acoustic scattering problems. Part 1: Dirichlet boundary conditions, Int. J. Numer. Methods Eng. 54 (2002) 1309–1332.
[6] U. Hetmaniuk, C. Farhat, A fictitious domain decomposition method for the solution of partially axisymmetric acoustic scattering problems. Part 2: Neumann boundary conditions, Int. J. Numer. Methods Eng. 58 (2003) 63–81.
[7] R. Glowinski, T.-W. Pan, J. Periaux, A fictitious domain method for external incompressible viscous flow modelled by Navier–Stokes equations, Comput. Methods Appl. Mech. Eng. 112 (1994) 133–148.
[8] R. Glowinski, T.-W. Pan, T.I. Hesla, D.D. Joseph, J. Periaux, A fictitious domain approach to the direct numerical simulation of incompressible viscous flow past moving rigid bodies: application to particulate flow, J. Comput. Phys. 169 (2001) 363–427.
[9] K.M. Arthurs, L.C. Moore, C.S. Peskin, E. Pitman, H.E. Layton, Modeling arteriolar flow and mass transport using the immersed boundary method, J. Comput. Phys. 147 (2) (1998) 402–440.
[10] A.M. Roma, C.S. Peskin, M.J. Berger, An adaptive version of the immersed boundary method, J. Comput. Phys. 153 (2) (1999) 509–534.
[11] F. Baaijens, A fictitious domain/mortar element method for fluid–structure interaction, Int. J. Numer. Methods Fluids 35 (2001) 743–761.
[12] I. Babuska, The finite element method with Lagrangian multipliers, Numer. Math. 20 (1973) 179–192.
[13] J. Pitkaranta, Boundary subspaces for the finite element method with Lagrange multipliers, Numer. Math. 33 (1979) 273–289.
[14] H.J. Barbosa, T.J.R. Hughes, The finite element method with lagrange multipliers on the boundary: Circumventing the Babuka–Brezzi condition, Comput. Methods Appl. Mech. Eng. 85 (1991) 109–128.
[15] J. Haslinger, J.F. Maitre, L. Tomas, Fictitious domains methods with distributed Lagrange multipliers. Part I: Application to the solution of elliptic state problems, Math. Models Methods Appl. Sci. 11 (3) (2001) 521–547.
[16] Z. Yu, A DLM/FD method for fluid/flexible-body interactions, J. Comput. Phys. 207 (2005) 1–27.
[17] C.S. Peskin, The immersed boundary method, Acta Numer. 11 (2002) 479–517.
[18] X. Wang, From immersed boundary method to immersed continuum method, Int. J. Multiscale Comp. Eng. 4 (2006) 127–145.
[19] R.J. Leveque, Z. Li, Immersed interface methods for stokes flow with elastic boundaries or surface tension, SIAM J. Sci. Comput. 18 (1997) 709–735.
[20] B. Maury, A fat boundary method for the Poisson equation in a domain with holes, J. Sci. Comput. 16 (3) (2001) 319–339.
[21] O.C. Zienkiewicz, R.L. Taylor, The Finite Element Method, fifth ed., Oxford, 2000.

[22] I. Ramiere, P. Angot, M. Belliard, Fictitious domain methods to solve convection–diffusion problems with general boundary conditions, in: 17th AIAA Computational Fluid Dynamics Conference, No. 2005-4709, Toronto, Canada, 2005.
[23] L. Zhang, A. Gerstenberger, X. Wang, W. Liu, Immersed finite element method, Comput. Methods Appl. Mech. Eng. 193 (2004) 2015–2067.
[24] S. Dong, D. Liu, M.R. Maxey, G. Karniadakis, Spectral distributed Lagrange multiplier method: algorithm and benchmark tests, J. Comput. Phys. 195 (2004) 695–717.
[25] R. Glowinski, T.-W. Pan, T.I. Hesla, D. Joseph, A distributed Lagrange multiplier/fictitious domain method for particulate flows, Int. J. Multiphase Flow 25 (1997) 755–794.
[26] L. Parussini, Fictitious domain approach for spectral/hp element method, CMES 17 (2) (2007) 95–114.
[27] J.P. Pontaza, J.N. Reddy, Spectral/hp least-squares finite element formulation for Navier–Stokes equations, J. Comput. Phys. 190 (2003) 523–549.
[28] M.M.J. Proot, M.I. Gerritsma, A Least-Squares Spectral Element formulation for the Stokes problem, J. Sci. Comput. 17 (2002) 285–296.
[29] L. Parussini, Fictitious domain approach via Lagrange multipliers with least squares spectral element method, J. Sci. Comput. doi: 10.1007/s10915-008-9212-x (online).
[30] R.A.E. Makinen, T. Rossi, J. Toivanen, A moving mesh fictitious domain approach for shape optimization problems, Math. Modeling Numer. Anal. 34 (1) (2000) 31–45.
[31] P.B. Bochev, M.D. Gunzburger, Finite element methods of least-squares type, SIAM Rev. 40 (1998) 789.
[32] H. Lomax, T. Pulliam, D. Zingg, Fundamentals of Computational Fluid Dynamics, Springer, Berlin, 2001.
[33] G.E. Karniadakis, S.J. Sherwin, Spectral/hp Element Methods for CFD, Oxford University Press, Oxford, 1999.
[34] M. Gerritsma, B.D. Maerschalck, The least-squares spectral element method, in: VKI Lecture Series 2006-01: 34th CFD – Higher Order Discretization Methods (ISSN: 0377-8312), Von Karman Institute, Bruxelles, 2006.
[35] C.-Y. Wu, X.-Y. Liu, A. Scarpas, X.-R. Ge, Spectral element approach for forward models of 3d layered pavement, CMES 12 (2) (2006) 149–157.
[36] D. Komatitsch, J.-P. Vilotte, The spectral element method: an efficient tool to simulate the seismic response of 2d and 3d geological structures, Bull. Seismol. Soc. Am. 88 (1998) 368–392.
[37] M. Abramowitz, I.A. Stegun, Handbook of Mathematical Functions, Dover Publications, New York, 1972.
[38] F. Brezzi, M. Fortin, Mixed and Hybrid Finite Element Methods of Springer Series in Computational Mathematics, Vol. 15, Springer-Verlag, 1991.
[39] C. Canuto, T. Kozubek, A fictitious domain approach to the numerical solution of PDEs in stochastic domains, Numer. Math. 107 (2007) 257–293.
[40] V. Girault, R. Glowinski, Error analysis of a fictitious domain method applied to a Dirichlet problem, Jpn. J. Ind. Appl. Math. 12 (1995) 487–514.
[41] R. Stenberg, On some techniques for approximating boundary conditions in the finite element method, J. Comput. Appl. Math. 63 (1995) 139–148.
[42] P.B. Bochev, R.B. Lehoucq, Regularization and stabilization of discrete saddle-point variational problems, Electron. Trans. Numer. Anal. 22 (2006) 97–113.
[43] A.S. Grove, F.H. Shair, E.E. Petersen, A. Acrivos, An experimental investigation of the steady separated flow past a circular cylinder, J. Fluid Mech. 19 (1964) 60.
[44] D.J. Tritton, Experiments on the flow past a circular cylinder at low Reynolds number, J. Fluid Mech. 6 (1959) 547.
[45] C. Wieselsberger, New data on the laws of fluid resistance, NACA TN 84.
[46] S.C.R. Dennis, G.-Z. Chang, Numerical solution for steady flow past a circular cylinder at Reynolds numbers up to 100, J. Fluid Mech. 42 (1970) 471.
[47] B. Fornberg, A numerical study of steady viscous flow past a circular cylinder, J. Fluid Mech. 98 (1980) 819.
[48] T. Ye, R. Mittal, H.S. Udaykumar, W. Shyy, An accurate Cartesian grid method for viscous incompressible flows with complex immersed boundaries, J. Comput. Phys. 156 (1999) 209–240.
[49] H. Takami, H.B. Keller, Steady two-dimensional viscous flow of an incompressible fluid past a circular cylinder, Phys. Fluids (Suppl. II) (1969) 51.
[50] F. Nieuwstadt, H.B. Keller, Viscous flow past circular cylinders, Comput. Fluids 1 (1973) 59.
[51] S.C.R. Dennis, The numerical solution of the vorticity transport equation, in: H. Cabannes, R. Tewam (Eds.), Proc. 3rd Int. Conf. on Numerical Methods in Fluid Mech., vol. 2, Lecture Notes in Physics, vol. 19, Springer, 1973, p. 120.
[52] S.E. Rogers, D. Kwak, An upwind differencing scheme for the time-accurate incompressible Navier–Stokes equations, Technical Memorandum AIAA PAPER 88-2583, NASA Center: Ames Research Center, 1988.
[53] S.Y. Tuann, M.D. Olson, Numerical studies of the flow around a circular cylinder by finite element method, Comput. Fluids 6 (1978) 219.
[54] M. Braza, P. Chassaing, H.H. Minh, Numerical study and physical analysis of the pressure and velocity fields in the near wake of a circular cylinder, J. Fluid Mech. 165 (1986) 79–130.
[55] P.L. Ta, Etude numerique de l'ecoulement d'un fluide visqueux incompressible autour d'un cylindre fixe ou en rotation effet magnus, J. Mecanique 14 (1975) 109.
[56] M. Coutanceau, R. Bouard, Experimental determination of the main features of the viscous hydrodynamic field in the wake of a circular cylinder in a uniform stream, J. Fluid Mech. 79 (1977) 231–239.
[57] T. Lee, D. Mateescu, Experimental and numerical investigation of 2-d backward-facing step flow, J. Fluids Struct. 12 (6) (1998) 703–716.
[58] B. Armaly, F. Durst, J. Pereira, B. Schonung, Experimental and theoretical investigation of backward-facing step flow, J. Fluid Mech. 127 (1983) 473–496.
[59] D.K. Gartling, A test problem for outflow boundary conditions – flow over a backward-facing step, Int. J. Numer. Methods Fluids 11 (1990) 953–967.
[60] J. Kim, P. Moin, Application of a fractional-step method to incompressible Navier–Stokes equations, J. Comput. Phys. 59 (1985) 308–323.
[61] J. Sohn, Evaluation of FIDAP on some classical laminar and turbulent benchmarks, Int. J. Numer. Methods Fluids 8 (1988) 1469–1490.